Assimilating long-term hydrographic information into an eddy-permitting model of the North Atlantic

D. G. Wright,[1] K. R. Thompson,[2] and Y. Lu[1]

Received 3 August 2005; revised 22 May 2006; accepted 13 June 2006; published 15 September 2006.

[1] The utility of a new technique for assimilating long-term hydrographic information into eddy-permitting ocean models is demonstrated using the Parallel Ocean Program (POP) applied to the North Atlantic. Robust diagnostic and standard prognostic simulations of the North Atlantic yield results similar to those obtained in earlier studies and the differences between them emphasize the need for data assimilation. The basic idea of the new technique is to add correction terms to the model equations that directly influence the model solution only in prescribed frequency and wave number bands, leaving the variations outside of these bands free to evolve prognostically. For this reason the technique is referred to as spectral nudging. We consider two approaches for constraining eddy-permitting models based on observed long-term hydrographic conditions. In the first approach, the model's temperature and salinity climatologies are spectrally nudged toward observed values using restoring terms in the tracer equations; in the second, correction terms are added to the momentum equations. Both approaches result in significant improvements in the model's climatology, as expected. Both approaches also result in more realistic meso-scale eddy fields. However, for the simulations considered here, spectral nudging in the tracer equations generally provides better results than nudging in the momentum equations. An examination of the relationship between the two approaches reveals that this result might be expected to also occur in other model simulations but this is achieved at the cost of increased constraints placed on model dynamics within the nudged frequency and wave number bands.

Citation: Wright, D. G., K. R. Thompson, and Y. Lu (2006), Assimilating long-term hydrographic information into an eddy-permitting model of the North Atlantic, *J. Geophys. Res.*, *111*, C09022, doi:10.1029/2005JC003200.

1. Introduction

[2] There have been many modeling studies focused on the North Atlantic over recent decades. The early diagnostic simulations provided large-scale circulation fields that were generally consistent with known features [e.g., *Sarmiento and Bryan*, 1982; *Mellor et al.*, 1982; *Greatbatch et al.*, 1991; *Bogden et al.*, 1993]. However, in such studies the temperature and salinity fields are required to remain close to the observations with the result that eddy and other variability not represented in the observed climatology is suppressed. Further, the presence of artificial sources and sinks can remove static instabilities, so it is unlikely that the simple diagnostic approach will provide a reliable representation of convective mixing; this can be a particular problem for investigations involving other tracers that are affected by this process, including studies of biological productivity.

[3] Prognostic calculations determine T-S fields as part of the solution to the model equations. Consequently, to achieve a useful representation of the real world, these models must more accurately represent the dynamical processes that control the evolution of the tracer fields. For non-eddy permitting models the effects of eddies and other unresolved processes are included through some form of parameterization while eddy-permitting models attempt to explicitly represent smaller scales and their interactions with the larger scales. Much has been learned from such models on both global and regional scales [e.g., *Semtner and Chervin*, 1988; *Webb et al.*, 1991; *Stammer et al.*, 1996; *DYNAMO Group*, 1997], but as *Dengg et al.* [1996] discuss, these models can also exhibit major shortcomings. Of relevance to the present study is the fact that Gulf Stream separation is often unrealistic, a particularly vexing problem for regional studies focused on the northwest Atlantic.

[4] Recent studies have demonstrated significant improvements when the horizontal resolution is increased to one sixth of a degree [see, e.g., *Chao et al.*, 1996; *Dietrich et al.*, 2004] and even greater improvements when the resolution is increased to a tenth of a degree or less [e.g., *Smith et al.*, 2000]. Presently, basin to global scale models with 10 km resolution are feasible at a few major laboratories but such model studies require major computer facilities. Further, even at this resolution, problems such as unrealistic Gulf

[1]Ocean Circulation Section, Bedford Institute of Oceanography, Dartmouth, Nova Scotia, Canada.
[2]Department of Oceanography, Dalhousie University, Halifax, Nova Scotia, Canada.

0148-0227/06/2005JC003200

Table 1. Differences Between Model Simulations[a]

Run Description	Location of Nudging	Frequencies Nudged	Wavelengths Nudged
Diagnostic	T and S equations	$\omega < 1/\tau_2$	$>12\ \Delta x$
Prognostic	None	N/A	N/A
Tracer-nudging	T and S equations	Mean and annual	$>12\ \Delta x$
Semi-prognostic	Momentum equation	Mean and annual	$>12\ \Delta x$

[a]Summary of the differences between the four runs discussed. Note that in all cases, identical nudges are applied in the sponge layers and on the shelves as described in the text. The only difference between the various runs is the type of nudging applied in the interior of the model. The final column indicates the wavelength beyond which nudging is reduced by more than a factor of 2. For a reduction by more than a factor of 5, the cutoff wavelength decreases to $8\ \Delta x$.

Stream separation can persist [e.g., *Maltrud and McClean*, 2005]. Thus, although such models are capable of simulating realistic variability, they may still suffer from some bias problems similar to those encountered in coarser resolution eddy-permitting models.

[5] To examine the influence of both mean conditions and eddy variability within a common, realistic and computationally affordable framework, we develop a methodology that combines the positive attributes of diagnostic and prognostic models. That is, we develop a method by which the model's large-scale climatology is constrained to be consistent with the observed climatology while the eddy variability is free to evolve according to the model dynamics and external forcing. Such a method is clearly most useful when we are concerned with the influence of both the mean state and the variability in hydrographic and circulation conditions, but the processes that are responsible for maintaining the climatology are not of immediate concern. Understanding the evolution of passive scalars and the variability in biological productivity are two important problems of this type.

[6] *Thompson et al.* [2006] (henceforth TWLD) have recently proposed a method that can achieve the goal discussed above. The method allows the user to restore the model state toward observed conditions in selected frequency and wave number bands; outside of these bands the model is free to evolve prognostically. For these reasons the method is referred to as spectral nudging. TWLD suggest that spectral nudging may be particularly useful for developing operational forecasting capacity using eddy-permitting models combined with other methods to assimilate observational information on eddy variability.

[7] We emphasize that both the observations and the models are imperfect. However, the observations provide valuable information on the mean state of the oceans that models have difficulty reproducing and the models provide information on the variability that the observations cannot resolve. Data assimilation in general, and the approach of TWLD in particular, take advantage of the strengths of each.

[8] In this study we examine two different forms of spectral-nudging in a model of the North Atlantic. In the first case, we add restoring terms to the tracer equations to nudge the T-S climatology of the model toward that estimated from observations (henceforth referred to as "tracer-nudging"). In the second approach, referred to as the "semi-prognostic" method, a generalized nudging term is added to the momentum equations. *Eden et al.* [2003] note that the original semi-prognostic method introduced by *Sheng et al.* [2001] has the disadvantages that wave properties are distorted and eddy variability is strongly suppressed. They use time-averaged model-data differences to determine the additional term in the momentum equation and show that this allows waves and eddy variability to develop more realistically. Here, we combine the original semi-prognostic method with the idea of spectral-nudging so that only very slowly varying misfits between the model and observed climatologies contribute to the term added to the momentum equation. This permits the eddy variability to evolve according to the model dynamics.

[9] The basic model, the model domain, parameterizations and forcing fields are discussed in section 2. In section 3, a robust diagnostic simulation based on a recently developed climatology is discussed and, in section 4, results are compared with those obtained from a standard prognostic integration; the latter results are included primarily to emphasize the need for data assimilation. In section 5 we review the basic idea of spectral-nudging and discuss its application through the addition of nudging terms in either the tracer or the momentum equations. The results of the two nudging approaches are compared and discussed in section 6. In section 7 we examine the nudges applied to the model in the tracer equations and how they relate to advective and diffusive flux divergences. In the final section we summarize results and discuss some issues that warrant further investigation.

2. Basic Model Setup

[10] In this section, we discuss only those model choices that are common to all of the simulations. The features that distinguish the various runs are summarized in Table 1.

[11] The model is based on the Parallel Ocean Program (POP) code developed at Los Alamos [*Smith et al.*, 2000]. The model domain extends from 7°N to 67°N and from 99°W to 20°E (Figure 1). The horizontal resolution is 1/3° in longitude and varies in latitude such that all grid cells are approximately square (i.e., $\Delta y = a\Delta\phi = a\cos\phi\,\Delta\lambda = \Delta x$, where a is the Earth's radius and ϕ and λ are latitude and longitude, respectively). The resulting horizontal grid spacing is 37 km at the southern boundary and 14 km at the northern boundary. In the vertical, there are 23 layers with thicknesses of 10, 10, 15, 20, 20, 25, 35, 50, 75, 100, 150, 200, 275, 350, 415, 450, 500, 500, 500, 500, 500, 500 and 500 m. The maximum model depth is 5700 m.

[12] Unresolved horizontal mixing is represented by biharmonic damping for both momentum and tracers, with the tracer diffusion chosen to be 8 times smaller than the momentum diffusion in order to minimize the "Veronis effect" [*Veronis*, 1975; *Böning et al.*, 1995, 1996]. The momentum diffusion coefficient, A_m, equals $-1.8 \cdot 10^{19}\ \mathrm{cm}^4\ \mathrm{s}^{-1}$ at the southern boundary of the model, so that the Munk layer is at best marginally resolved at this location ($(A_m/\beta)^{1/5} \sim 25$ km). A_m decreases northward proportional to $[\Delta x \Delta y]^{1.5}$, so the

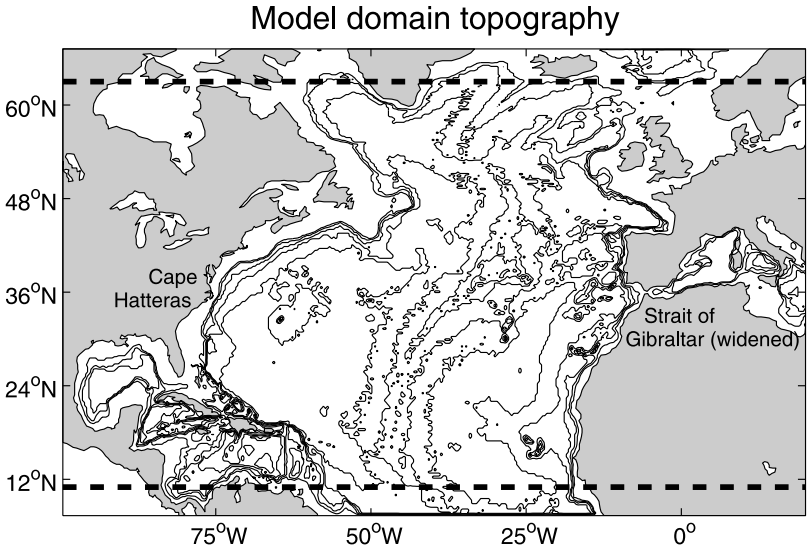

Figure 1. The model domain and bottom depth contours at 1000 m intervals. The inner edges of the "sponge layers" within which the restoring to climatology is increased to account for external influences are delineated by dashed lines parallel to the northern and southern boundaries.

Munk layer (with width $\propto \cos^{2/5}(\phi)$) decreases less quickly than the grid size ($\propto \cos\phi$) and becomes somewhat better resolved at higher latitudes. The vertical mixing is represented using the K-profile parameterization of *Large et al.* [1994]; wind stress and Richardson number dependent mixing are included but double diffusive mixing is neglected. Static instabilities are eliminated by increasing the vertical diffusion coefficients for both tracers and momentum to 2000 $cm^2\ s^{-1}$ between unstable cells.

[13] Numerous authors [e.g., *Doscher et al.*, 1994; *Gerdes and Koberle*, 1995; *DYNAMO Group*, 1997; *Lohmann*, 1998] have discussed the importance of including realistic conditions at the north and south boundaries. We employ so-called sponge layers adjacent to the northern and southern boundaries that are 4° wide (Figure 1). Within the sponge layers, the model's temperature and salinity are restored to climatological estimates developed by I. Yashayaev at the Bedford Institute of Oceanography (see http://www.mar.dfo-mpo.gc.ca/science/ocean/woce/climatology/naclimatology.htm). The restoring timescale varies from 4 days at the extremities of the model domain to infinity at the interior edges of the sponge layers (the inverse of the timescale varies linearly). Within the 3 grid cells nearest to the northern and southern boundaries, the advection of tracer fields is set to zero, and within the next 3 grid cells the advection is increased to normal values. This approach allows observed conditions to be easily maintained even though there is unrealistically strong upwelling/downwelling in these regions. We emphasize, however, that conditions within about two degrees of the boundaries should be thought of as part of the specified boundary conditions rather than part of the model solution.

[14] For the spatial scales resolved by our grid, and for timescales of a few days or more, thermal wind gives a good estimate of the vertical current shear, so both the water mass properties and the vertical shear inside of the sponge layers are strongly nudged toward observational estimates. However, we note that sponge layers do not fully account for the interactions with unresolved regions [see, e.g., *Klink*, 1995] and this is clearly a model limitation. We reduce the problems associated with the open boundaries by specifying the depth-integrated flow normal to the boundaries according to a simple radiation condition of the form $V = V^S - 0.9\,(\Delta y/\Delta t)\,(\eta - \eta^S)$, where Δy and Δt are the model's horizontal grid size and time step respectively, and superscript S refers to values that are specified. This boundary condition is directly analogous to the form used by *Lu et al.* [2001]. The radiation phase speed, $0.9\Delta y/\Delta t$, is less than the external gravity wave phase speed almost everywhere in the model domain, but this radiation condition eliminates 90% of the discrepancy between η and η^S on each time step without creating numerical instabilities. In the present implementation, V^S and η^S are obtained from the monthly climatology of a data assimilative ocean model with 1° horizontal resolution that covers the global ocean except for the Arctic Ocean [*Kohl et al.*, 2006]. For consistency, we also merge the temperature and salinity from the 1° model results with the Yashayaev climatology over 5 degree bands adjacent to the boundaries, (i.e., we use α (Yashayaev) + $(1-\alpha)$ (1° Model Climatology), where $\alpha = 1$ over the bulk of the domain but linearly decreases to zero over 5° bands adjacent to the open boundaries). Obviously, our treatment of the open boundaries is not perfect. Any remaining problems, including those in the model interior, will be reduced by the spectral nudging.

[15] The model depths are based on the topography of *Smith and Sandwell* [1994, 1997]. Initial model depths are estimated by taking the mean of the *Smith and Sandwell* [1997] depth over each horizontal grid cell and then choosing the number of grid cells in the vertical to give the best estimate of this depth. The depths over the northern sills, through the Caribbean and in the Strait of Gibraltar are then modified so that the passages in these regions are at least two cells wide to allow throughflow on the B-grid.

[16] The model is initialized in a state of rest with temperature and salinity set to the January climatology of Yashayaev. Surface heat, momentum and freshwater fluxes

are specified according to the monthly climatology constructed from the NCEP reanalysis for the period 1948–2001. A third order polynomial fit to the four nearest monthly estimates is used to interpolate to specific model times. Following *Barnier et al.* [1995], the surface heat flux is specified as the sum of the NCEP net surface heat flux and a restoring term; the spatially and temporally varying restoring coefficient was obtained from the monthly climatology of *da Silva et al.* [1994]. The surface boundary condition for salinity is analogous to the heat flux formulation with the virtual salt flux determined from precipitation minus evaporation fields from the NCEP reanalysis plus a term that restores the model's surface salinity toward the observed climatology on a timescale of 100 days. To crudely represent the influence of river runoff onto the shelves, the salinity is restored to the observed climatology on a timescale of 5 days where the water depth is less than 50 m. Tests show that this has little impact on our solutions in the deep ocean.

3. Robust Diagnostic Results and an Adjusted Climatology

[17] The simplest way to force a model's temperature and salinity fields to agree with observations is to directly insert them into the model. However, this can result in unrealistic model features, particularly in the vertical velocity, depth integrated transport stream function and the zonally integrated overturning stream function. Such unrealistic features can be attributed to model-data inconsistencies related to several different problems: sparse data and imperfect interpolation and extrapolation routines; measurement errors; inadequate data to fully separate temporal variability from spatial gradients; and inconsistencies between the observed climatology and the approximate bottom topography and dynamics used in the model. The latter point is particularly important because inconsistencies between the density field and the bottom topography result in errors in the JEBAR term [e.g., *Sarkisyan and Ivanov*, 1971; *Mertz and Wright*, 1992; *Slordal and Weber*, 1996] that can cause large errors in the model's velocity.

[18] We now introduce an approach that will allow small adjustments to the observed climatology in order to reduce inconsistencies with the model's approximate representations of bathymetry and dynamics. The approach is similar to the "robust diagnostic" approach of *Sarmiento and Bryan* [1982] and the 30-day prognostic adjustments used by *Ezer and Mellor* [1994]. In addition to reducing model-data inconsistencies, this approach will also (1) provide a convenient benchmark against which to compare results obtained with spectral nudging, and (2) lead to an "in-line" way of determining a dynamically adjusted climatology to which we will spectrally nudge.

[19] Let (T^{cl}, S^{cl}) represent observed temperature and salinity climatologies interpolated onto the model grid. We wish to determine modified climatologies, denoted as (T^*, S^*), that are more consistent with the model's representation of the bathymetry and dynamical processes but are still close to (T^{cl}, S^{cl}). We focus below on T^* but the adjustment of S^* is analogous.

[20] Let F(x, y, z, t) denote the sum of all forcing terms influencing the evolution of T^* at a given grid point, including advection, diffusion, convection and external forcing. The standard prognostic update is then

$$T^{*f}_{n+1} = T^{*}_{n-1} + 2\Delta t \cdot F, \tag{1}$$

where the superscript f indicates a prognostic model forecast and the factor of 2 multiplying Δt arises from the use of a leapfrog time stepping scheme. According to the robust diagnostic approach, a simple nudging term is added to complete the update of T^*_{n+1}:

$$T^{*}_{n+1} = T^{*f}_{n+1} + \left\langle \frac{2\Delta t}{\tau_1}\left(T^{cl}_{n+1} - T^{*f}_{n+1}\right)\right\rangle, \tag{2}$$

where the angled brackets represent a spatial smoothing operation that filters out small-scale variability (see Table 1). All larger scale variability is nudged toward the climatology with a timescale τ_1.

[21] The restoring time τ_1 can be specified such that some areas are more tightly constrained by the observations than others; our choices are guided by a combination of physical reasoning and experimentation. Initially, we included nudging terms over the entire domain with τ_1 increasing from 20 days in the upper 55 m to 77 days at the bottom. Experimentation shows that this is long enough for density adjustment to greatly diminish anomalous structures in the barotropic and overturning stream functions, but short enough that scales of 100 km or more are well-constrained almost everywhere. An exception occurs near Cape Hatteras where strong advection results in changes that are larger than the observational uncertainties in this region. Thus, to prevent unrealistic drift, the restoring time is reduced to 5 days at 72.5°E, 36°N and τ_1^{-1} decreases linearly with distance away from this location to the base value over 5° in both longitude and latitude. This local modification serves only to maintain the robust diagnostic results near the observations in this area. (In later sections we nudge the model's climatology toward an observed climatology that has been adjusted similar to the robust diagnostic results presented here. However, the nudging of the model climatology toward this observed climatology will not be increased in the region around Cape Hatteras.)

[22] To illustrate bulk properties of our solutions, the time-averaged stream functions for the depth-integrated flow,

$$\Psi_{BT}(\lambda,\phi) = \int_{\lambda_w}^{\lambda}\int_{-h(\lambda',\phi)}^{0} \bar{v}(\lambda',\phi,z)a\cos\phi\, dz\, d\lambda', \tag{3}$$

and the zonally integrated overturning circulation,

$$\Psi_{OT}(\phi,z) = \int_{\lambda_w}^{\lambda_e}\int_{z}^{0} \bar{v}(\lambda,\phi,z')a\cos\phi dz' d\lambda, \tag{4}$$

were determined for each model run. In the above formulae, the subscripts 'w' and 'e' indicate the western and eastern limits of the North Atlantic basin, z is the vertical coordinate with $z = 0$ at the resting location of the sea surface and $\bar{v}$ is the time-averaged meridional velocity component.

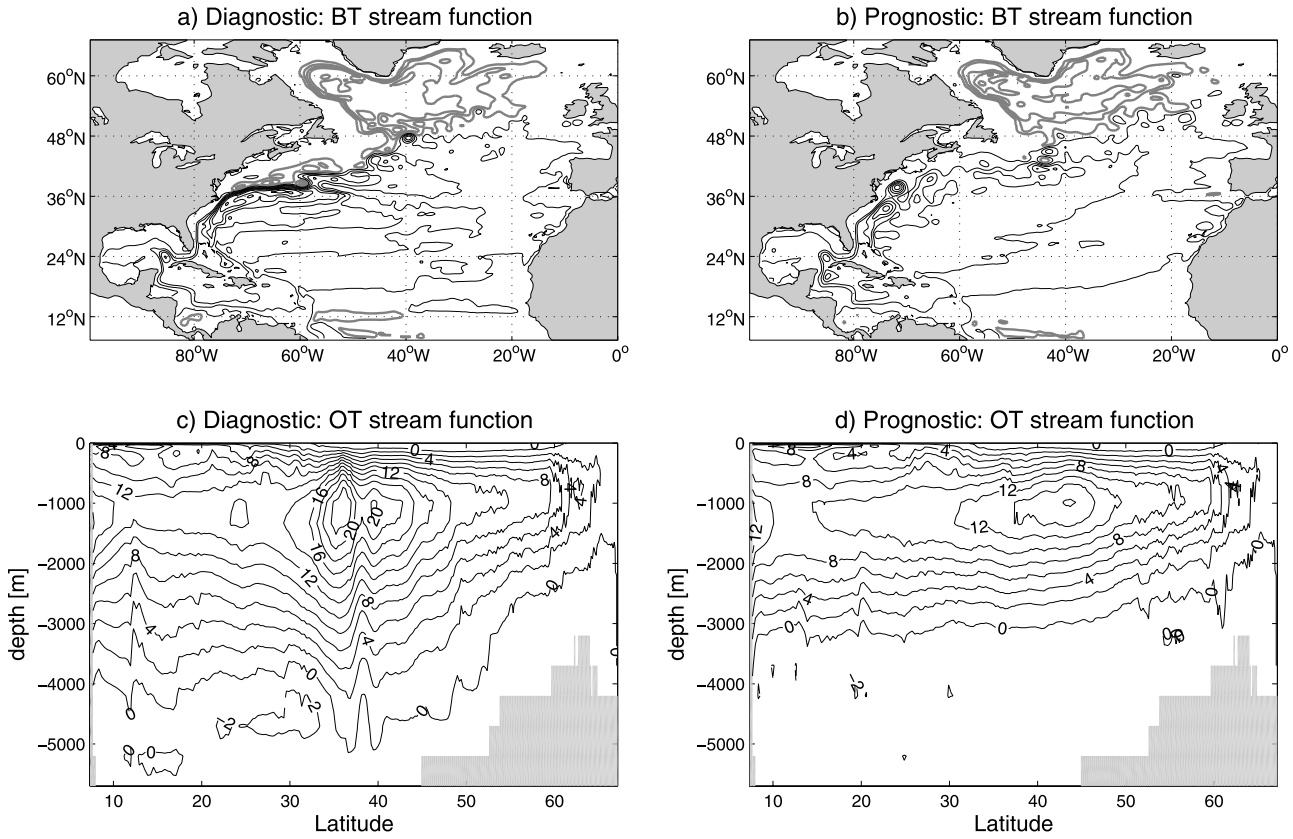

Figure 2. (a) Stream function for the depth-integrated flow averaged over the last 5 years of a 15-year robust diagnostic integration. (b) The corresponding stream function for the progostic run but from the last 5 years of a 30-year integration. (c) and (d) Zonally integrated overturning circulations corresponding to Figures 2a and 2b, respectively. Note that the model domain extends to 15°E but results are not shown to the east of 0° in Figures 2a and 2b (or subsequent plots of this form) in order to expand the region of interest. However, all zonal averages include the region between 0° and 15°E.

[23] Averages over the last 5 years of a 15-year robust diagnostic integration are shown in Figure 2 together with results obtained by averaging over the last five years of a 30-year prognostic integration. The annual averages of the robust diagnostic results change very little after the first year and are generally consistent with the corresponding results produced in previous studies. They are discussed in the next section along with the results of the prognostic simulation.

4. Prognostic Results and the Need for Data Assimilation

[24] *Willebrand et al.* [2001] provide examples of results obtained by the DYNAMO Group for prognostic integrations of three different models configured similarly to the model used in the present study. As expected, the results that we obtain with prognostic integration are most similar to those reported for the geopotential model MOM. Here, we show only a few results from our prognostic integration, primarily to review some of the problems encountered with models of this resolution. Model results during the first few months of integration are encouraging, but they degrade over time. Our interest here is in the solution that develops after several years of integration.

[25] Comparing Figure 2b with Figure 2a, it is obvious that the prognostic integration has drifted away from reality over the 30 years of integration. In particular, we note that the recirculations north and south of the Gulf Stream in the robust diagnostic calculation are almost absent in the prognostic calculation. Annual averages over the first few years of prognostic integration show that these features reduce substantially during the first two years of integration and are almost eliminated by the fourth year. As the northern recirculation collapses, a large time-varying anticyclonic circulation develops northeast of Cape Hatteras and the Gulf Stream weakens and shifts toward the slope along the Gulf of Maine and the Scotian Shelf. Consequently, the separation of the Gulf Stream near Cape Hatteras is very poorly represented in the prognostic integration.

[26] Comparing Ψ_{OT} from Figures 2c and 2d shows that the overturning has also changed dramatically, including a reduction in both the maximum value and the depth to which the overturning penetrates. Each of these changes reduces the climatically important meridional heat flux as discussed in section 6.

[27] The results shown in Figures 2b and 2d are typical of other prognostic calculations with similar horizontal resolution [e.g., *Beckmann et al.*, 1994; *Dengg et al.*, 1996; *Smith et al.*, 2000; *Willebrand et al.*, 2001]. Without increasing model resolution, and in the absence of improved parameterizations and forcing terms, some form of data assimilation is required to maintain the models' climatologies to be consistent with observations.

5. Spectral-Nudging in the Tracer and Momentum Equations

[28] In this section we briefly review the essence of the method introduced by TWLD for assimilating climatological data into an eddy-permitting ocean model and discuss how this technique can be applied for nudging in either the tracer or the momentum equations.

5.1. Spectral Nudging in the Tracer Equations

[29] We begin by considering the standard robust diagnostic method for restoring temperature and salinity toward observed values:

$$\frac{\partial T}{\partial t} = -\nabla \cdot (\boldsymbol{u}T) + \nabla^2\left(K_H \nabla^2 T\right) + \frac{\partial}{\partial z}\left(K_V \frac{\partial T}{\partial z}\right) + N^T \quad (5a)$$

$$\frac{\partial S}{\partial t} = -\nabla \cdot (\boldsymbol{u}S) + \nabla^2\left(K_H \nabla^2 S\right) + \frac{\partial}{\partial z}\left(K_V \frac{\partial S}{\partial z}\right) + N^S \quad (5b)$$

where $N^{(T,S)} = \tau^{-1}[(T^* - T), (S^* - S)]$, τ is a relaxation timescale and T^*, S^* denote the temperature and salinity climatologies to which we nudge. Below, we drop the superscripts T and S on the nudges, but it is to be understood that each reference to N refers to nudging terms in both the temperature and the salinity equations.

[30] A well-known drawback of the simple approach described above is that strong restoring is required to obtain a close match between T and T^* but this suppresses variability that is not represented by T^* [*Pierce*, 1996; *Woodgate and Killworth*, 1997]. The essence of the spectral nudging approach is to replace the nudging term, N, by $\langle\widetilde{N}\rangle$, where the tilde represents a temporal filter and the angled brackets represent a spatial filter so that only selected frequencies and wave numbers remain in the nudging terms. Thus, the equations remain exactly the same but the definitions of N^T and N^S are modified to include spatial and temporal filtering. These filters should be chosen so that the frequencies and wave numbers that are constrained by the nudging are resolved by the observed climatology. The properties of both temporal and spatial filters can vary over the model domain if desired. TWLD describe an efficient, in-line temporal filter that can be used to pass energy within prescribed frequency bands. In their study the frequencies were centered on the climatological frequencies of 0, 1 and 2 cycle per year and the width of the bands was typically 1/5 cycle per year. In space TWLD used a 4th order lowpass Butterworth filter in ϕ and λ to suppress high wave number variability in the nudges. The same authors note that there is a related technique, also referred to as spectral nudging, that uses spatial filtering (but without temporal filtering) to help downscale large-scale atmospheric states using regional models [*von Storch et al.*, 2000, and references therein].

[31] We define our climatology to be composed of the mean plus annual cycle above 260 m depth and just the mean below 260 m. The temporally filtered version of N is updated independently at every grid cell of the model at a specified time interval. The updating interval could be chosen larger than the model time step, but the savings achieved by doing this are small, so we have updated $\widetilde{N}$ every model time step. For our spatial filter, we use 10 iterations of a 9-point weighted mean over the surrounding water points; the weights are of the form (1, 2, 1; 2, 4, 2; 1, 2, 1) divided by the sum of the weights over the water points. To reduce the associated CPU demand, spatial filtering is performed only once per day. Thus, while $\widetilde{N}$ is updated each time step, the temporally and spatially filtered nudges that are added to the model equations are only updated once per day. Since the nudges vary slowly in time, the error introduced by updating only once per day is negligible. By updating our nudges in this manner, the percentage increase in CPU associated with the combination of temporal and spatial filters remains below 25%. More sophisticated spatial filters (e.g., the Butterworth filter used by TWLD) could be used with little impact on CPU usage.

[32] It should be noted that either spatial or temporal filtering alone could be used to reduce the damping of eddy variability. Here we have chosen to use fairly weak spatial smoothing primarily to allow dynamical adjustment to reduce relatively small-scale model-data inconsistencies. Removal of eddy variability from the nudges is primarily accomplished by the temporal filter.

[33] The above approach has been successfully applied in a study of the North Pacific by *Stacey et al.* [2006]. However, a modification to this approach has been introduced by TWLD to reduce amplitude and phase shifts in the annual cycle and this modified approach will be used in the next section. An heuristic interpretation of the approach is presented below.

[34] In the approach introduced by TWLD, the fully updated form of T_{n+1} can be expressed as

$$T_{n+1} = T^f_{n+1} + \left\langle \tilde{T}^*_{n+1} - \tilde{T}^*_{n-1} \right\rangle - \left\langle \tilde{T}^f_{n+1} - \tilde{T}_{n-1} \right\rangle + \left\langle \frac{2\Delta t}{\tau_2}\left(\tilde{T}^*_n - \tilde{T}_n\right) \right\rangle, \quad (6)$$

where T^f_{n+1} is the prognostic forecast as in equation (1) and the remaining terms represent the corrective nudging. The first term in angled brackets gives the desired change over the leapfrog time step as estimated from T^* and the second term gives the change that the model experiences before the nudge is applied. Thus, the first two bracketed terms replace the change in T within the chosen frequency and wave number bands determined by the model dynamics with the corresponding change in T^*.

[35] Although the first two bracketed terms in (6) will ensure that the model climatology tracks the observed climatology, there is nothing in them to eliminate misfits that develop during the initial adjustment period when the time-filtered quantities are not well determined. That is, the temporal mean is in the null-space of this component of the nudge. Thus, to complete the update of T_{n+1} we add the final term in (6) which pulls $\langle\widetilde{T}\rangle$ directly toward $\langle\widetilde{T^*}\rangle$. Note

that it is possible for the final term in (6), proportional to the model-data misfit, to approach zero without the nudge also approaching zero. We specify a constant value of 40 days for τ_2 but our results are not sensitive to this value since this component of (6) decreases to a relatively small value.

5.2. Spectral Nudging in the Momentum Equations

[36] The semi-prognostic approach was originally introduced by *Sheng et al.* [2001] and later modified by *Eden et al.* [2003] and *Zhai et al.* [2004]. In this approach, the tracer equations are not altered, but a term of the form $-\rho^{-1}\nabla_H\langle\alpha(\widetilde{p'^{cl}} - \widetilde{p'})\rangle$ is added to the horizontal momentum equations. The quantity α is an adjustable parameter that can be chosen to minimize the model-data misfit, p' is the hydrostatic pressure relative to the surface, ∇_H is the horizontal gradient operator and the tilde and angled brackets again represent temporal and spatial filters. *Sheng et al.* [2001] did not include any filtering and used $\alpha = 0.5$, *Eden et al.* [2003] used either an annual mean over the previous year of integration or 3-year-averages of monthly values over a previous time interval as their time filter and again chose $\alpha = 0.5$, and *Zhai et al.* [2004] used a spatial filter that passes only scales in excess of 300 km without any time filtering and used $\alpha = 1.0$. In the simulations discussed in the next section that use the semi-prognostic approach, we use the exact same temporal and spatial filters as discussed above for the case of nudging applied in the tracer equations and we use $\alpha = 1.0$.

5.3. In Line Adjustment of the Climatology

[37] The T^* and S^* used in the above nudging approaches are essentially equivalent to the robust diagnostic results presented in section 3, but one modification was made in their determination in order to avoid a separate model run. We simply include 4 tracers in each model simulation: the first pair is potential temperature and salinity, T and S, and the second pair is the adjusted climatologies, T^* and S^*. Both sets of tracers are advected by the same velocity field, which is directly influenced by the density variations associated with T and S. Thus, T^* and S^* actually experience advection determined by the density field associated with T and S rather than that associated with the climatology. Eddy variability in T^* and S^* is significantly damped since the frequency content of the nudges applied to these variables is not filtered. However, advection by the full velocity field and the spatial filtering of the nudges still result in more variability than would be found in a standard robust diagnostic solution [*Sarmiento and Bryan*, 1982]. On the other hand, since only the annual cycle and long-term mean values of T^* and S^* will be used in the implementation of spectral-nudging, this variability is of little consequence for our purposes. As a shorthand notation, we will henceforth refer to T^* and S^* as robust diagnostic estimates of the observed climatology.

6. Model Results With Spectral Nudging

[38] In this section, results from the tracer nudging and the semi-prognostic methods are discussed and compared. The spectral approach is used in both cases and the model formulation is the same as that used for the prognostic calculations discussed above.

[39] Table 1 summarizes the distinguishing features of the robust diagnostic, prognostic and the two spectrally nudged runs. Robust diagnostic and prognostic results have been discussed in section 4. In the runs discussed in this section, spectral nudging is applied in the model interior, with the mean state nudged at all levels and the seasonal cycle nudged only above layer 10 (i.e., at depths less than 260 m below the sea surface where the seasonal cycle is well defined). The nudging terms are based on differences between the model climatology and T*, S* as discussed in section 5. There is no spectral nudging above layer 10 of the model within the Gulf of Mexico in either method. This change was required to permit realistic shedding and propagation of Loop Current eddies, presumably because neither our data coverage in the Gulf of Mexico nor our temporal and spatial filters are adequate to properly separate the influence of Loop Current eddies from the mean and annual cycle.

[40] As discussed in the previous sections, spatial and temporal filters are applied to the nudges to avoid damping eddy variability. Exactly the same filters are applied for both tracer-nudging and the semi-prognostic approach. The time-filter bandwidth (see TWLD for details) is set to the maximum of 2/t and 1/(3 years) where t is the length of time since the beginning of the model run. Thus, initially a broad range of frequencies are nudged resulting in an essentially diagnostic spin-up period. However, by year 6 the bandwidth within which nudging is applied is reduced to 1/(3 years) so that only frequencies near 0 and 1 cycle per year are strongly nudged; beyond year 6 periods shorter than six months are only very weakly constrained.

[41] Figure 3 shows the depth-integrated and overturning stream functions averaged over the last 5 years of two 30-year model runs for the two spectrally nudged calculations. Comparing these results to those shown in Figure 2 reveals that each of the nudging approaches has achieved our first goal of keeping the barotropic and overturning stream functions close to the results of the robust diagnostic calculation.

[42] The most striking improvements in comparison to the prognostic results are associated with the Gulf Stream: the Stream separates near Cape Hatteras, the recirculations north and south of the Stream are similar to the diagnostic results, and the unrealistic anticyclonic circulation that developed north-east of Cape Hatteras in the prognostic run does not develop with either approach. Other notable improvements are evident in the vicinity of the ''northwest corner'' (north of Flemish Cap), where a circulation similar to the diagnostic result is maintained, and near the tail of the Grand Bank where southward and westward flows of subpolar water are maintained inside of the Gulf Stream path.

[43] Figure 4 illustrates the influence of spectral nudging on the climatically important meridional heat flux. The thin solid line shows the results of the robust diagnostic calculation and the vertical bars indicate observational estimates with error bars. We do not expect perfect agreement between the model and observational estimates of the heat flux, but the degree of similarity is encouraging. The thick solid curve shows the time average over the final 5 years of the prognostic integration as an example of what we are trying to avoid; note the reduction in the ocean heat transport south of 40°N. Previous work [e.g., *Böning et al.*, 2001] has shown that the meridional heat flux in the Atlantic basin is nearly proportional to the strength of the meridional over-

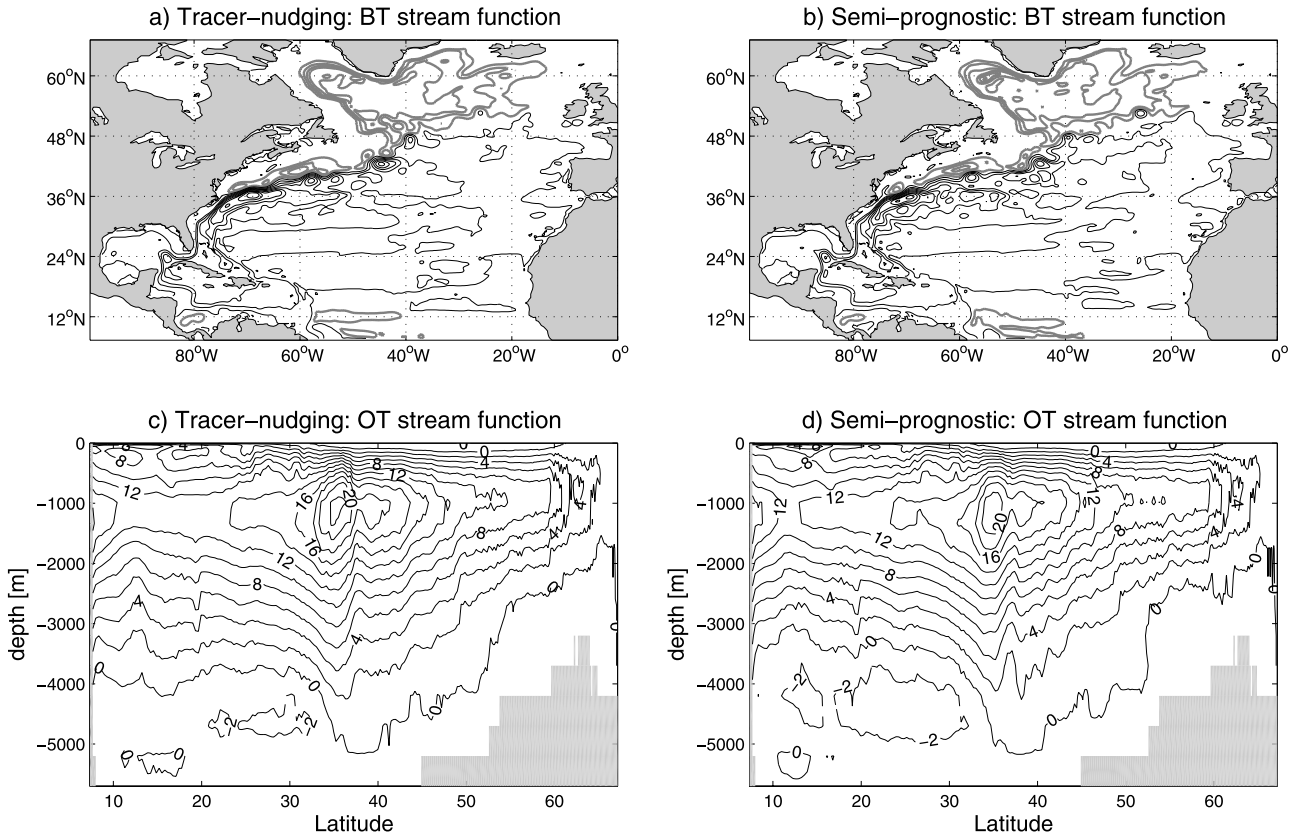

Figure 3. (a) Stream function for the depth-integrated flow averaged over the last 5 years of a 30 year integration with long-term hydrographic information assimilated through nudging in the temperature and salinity equations (the tracer-nudging approach). (b) The corresponding stream function obtained with nudging applied through the momentum equations (the semi-prognostic approach). (c) and (d) Zonally integrated overturning circulations corresponding to Figures 3a and 3b, respectively.

turning circulation, principally due to advection of warm surface water northward and the return of colder water southward at depth. The reduced heat flux in the prognostic integration is due to a reduction in the overall strength of the overturning circulation (Figure 2) together with increased deep temperatures and a southward return flow that occurs at shallower depths. The last two effects contribute to a reduced temperature contrast between the northward surface flow and the southward return flow at depth.

[44] One of our goals for the spectrally nudged runs was to maintain the annual mean heat flux near the values obtained with a robust diagnostic simulation while permitting variability determined by the model dynamics and forcing terms. The additional curves in Figure 4 are included to test whether or not this goal has been achieved. The dashed curve shows the time-average over the last 5 years of the run with nudging in the tracer equations. The diagnostic heat flux is reproduced very well and discrepancies relative to the observations are reduced as expected. The dot-dash line shows the results obtained using the semi-prognostic approach. We note that the differences from the robust diagnostic results are larger but the discrepancies relative to the observational estimates are similar to those obtained with tracer-nudging.

[45] In addition to eliminating long-term drift, spectral nudging is designed to permit variability that is governed by the model dynamics. Figure 5 shows the temporal changes in the domain-averaged kinetic energy (KE) from the robust diagnostic and prognostic runs as well as the two nudged runs. Annually averaged results for the diagnostic and prognostic solutions reach equilibrium levels of approximately 13 $(cm/s)^2$ and 17 $(cm/s)^2$. The tracer-nudging and semi-prognostic runs reach levels of approximately 22 $(cm/s)^2$ and 23.5 $(cm/s)^2$, respectively. For both the diagnostic and prognostic model runs, the basin-mean KE reaches its equilibrium value within about one year and experiences relatively small variations thereafter. For the two nudged runs, the KE increases reasonably smoothly over the first four years and then tends to stabilize with values oscillating between about 20 and 24 $(cm/s)^2$. The higher KE levels reached in the nudged runs are consistent with the maintenance of the Gulf Stream and the associated reservoir of available potential energy from which the eddies extract energy throughout the model simulations.

[46] Figure 6 shows the root-mean square sea level variability for prognostic (Figure 6a), tracer nudging (Figure 6b), the semi-prognostic run (Figure 6c) and an observational estimate (Figure 6d) based on gridded, delayed-mode satellite data from the Topex/Poseidon, Jason-1, ERS1/2 and

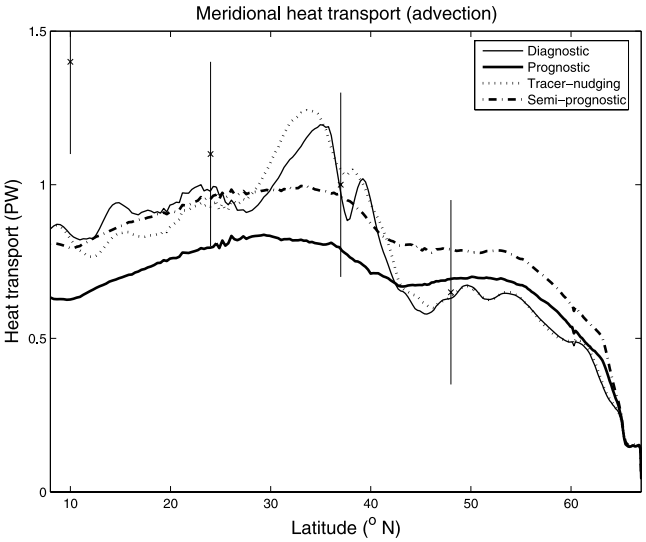

Figure 4. The time-averaged meridional heat flux carried by the North Atlantic estimated from the last 5 years of the robust diagnostic (thin solid line) and the prognostic (thick solid line) integrations together with recent observational estimates of this quantity. The dotted curve corresponds to the heat flux determined with tracer-nudging of temperature and salinity included as discussed in section 5 and the dot-dashed curve corresponds to the results obtained using the semi-prognostic approach discussed in section 6. Both of the latter results use the spectral nudging approach. The crosses and associated vertical lines show the inverse model estimates determined by *Macdonald* [1998]. Estimates by *Trenberth* [1998], based on atmospheric residual calculations, favor the lower end of Macdonald's error bars except at 24°N where the estimates overlap with the upper half of Macdonald's error bar.

ENVISAT satellite missions, generated and processed by the Space Oceanography Division of CLS (Collection Localisation Satellites) located in Toulouse, France [*Ducet et al.*, 2000]. Comparing Figures 6a, 6b and 6c with Figure 6d reveals that the sea level variability has been substantially improved by each form of spectral-nudging, but the results from tracer-nudging are closer to the observations.

[47] It should be noted that the monthly surface forcing does not include synoptic variability, so the model-simulated variability seen in Figure 6 is almost entirely due to nonlinear processes. Additional model simulations that are not shown here have been done with synoptic surface forcing for the period 1991–1999 using surface fluxes computed from the model's sea surface temperature and atmospheric daily mean parameters from the NCEP reanalysis. Including higher frequency variability in the surface forcing generates more high frequency variability on the shelves, but does not strongly influence the results for the open ocean beyond increasing slightly the background variance.

[48] Figure 7 shows snapshots of the temperature at level 6 (87 m) and level 16 (1975 m) after 15 years of integration for the diagnostic run and after 30 years of integration for each of the prognostic and the two nudged runs. Again, we see that spectral nudging has improved the representation of large-scale conditions in each of the runs. However, the large-scale results from the semi-prognostic approach are not as close to the benchmark robust diagnostic results as those obtained with tracer-nudging. This remains true if the snapshots are replaced by annual averages. We also note that the discrepancies in the northwest Atlantic obtained with the semi-prognostic approach are significantly larger than those presented in *Sheng et al.* [2001] using the original semi-prognostic method.

[49] Two possible explanations for the differences between our results and those of *Sheng et al.* [2001] have been investigated. First, we have rerun our model with the same climatology as used by *Sheng et al.* [2001]; this did not reduce our model bias with the semi-prognostic approach. A second possibility is that the smaller domain considered by Sheng et al. (see Figure 7h) results in greater control of the model solution through the lateral boundary conditions. To examine this influence, we added tracer-nudging in the region outside of the domain considered by *Sheng et al.* [2001]. This gives us the semi-prognostic solution within their model domain with the temperature, salinity and velocity through the open boundaries close to the results of our run with tracer-nudging. This reduced the discrepancy by about 30% over much of the water column, but still did not provide the agreement with observations obtained by *Sheng et al.* [2001]. We have not tried to force the reduced domain with exactly the same open boundary conditions as used by *Sheng et al.* [2001] which includes a stronger inflow through the northeastern boundary of the region. It is likely that this additional source of cold fresh water would further reduce the differences between our results and theirs. We also note that the model numerics used in the model of *Sheng et al.* [2001] are significantly different from those used in the POP model, including a different vertical mixing scheme, the use of an A-grid discretization and 4th order numerics in the model of *Sheng et al.* [2001]. Results presented later (section 7) lend support to the idea that such differences in model numerics may have significant impact on model results.

[50] Finally, it is of interest to further clarify the relation between the semi-prognostic approach and the more standard tracer-nudging approach. We first note that the semi-prognostic momentum equations differ from the usual Eulerian equations of motion through the addition of a pressure correction term that depends on the discrepancy between the model and the observed density fields. The addition of this term means that the velocity occurring in the semi-prognostic equations, $\boldsymbol{u}_{SP}$, can be written as $\boldsymbol{u} + \boldsymbol{u}_*$, where $\boldsymbol{u} = (u, v, w)$ is the standard Eulerian velocity associated with the hydrostatic pressure gradient determined by the model's density field and $\boldsymbol{u}_* = (u_*, v_*, w_*)$ represents the additional contribution associated with the correction terms in the semi-prognostic momentum equations governing $\boldsymbol{u}_{sp}$. Noting that the vertical viscosity depends on the model velocity field through the Richardson number dependent mixing term, we also write $A_V = A_V^0 + A_V^*$. Substituting $\boldsymbol{u}_{sp} = \boldsymbol{u} + \boldsymbol{u}_*$ and $A_V = A_V^0 + A_V^*$ into the semi-prognostic momentum equations and then subtracting the standard momentum equations for $\boldsymbol{u}$, one can easily derive equations for $\boldsymbol{u}_*$. These equations differ from the standard momentum equations in that the pressure gradient term is replaced by the pressure gradient adjustment term and there are addi-

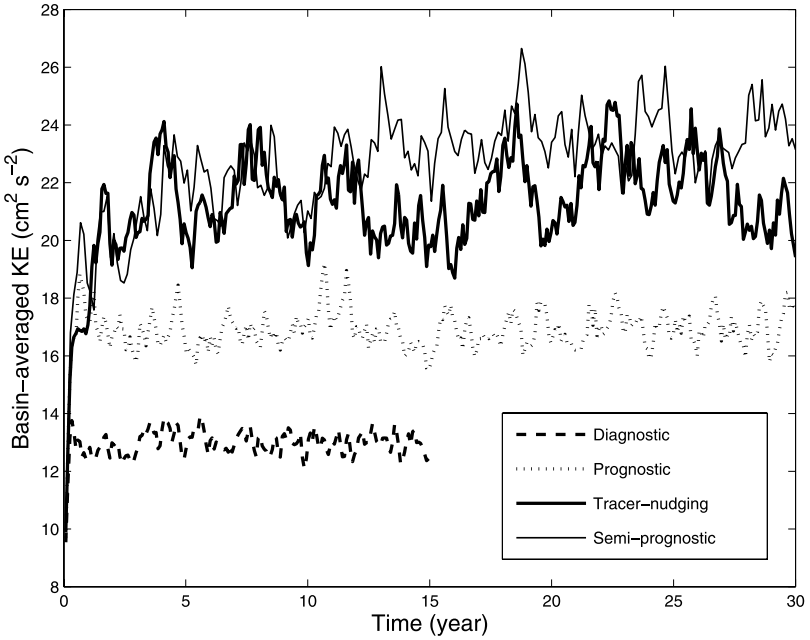

Figure 5. Time series of the domain-averaged kinetic energy for the robust diagnostic, prognostic and nudged model runs.

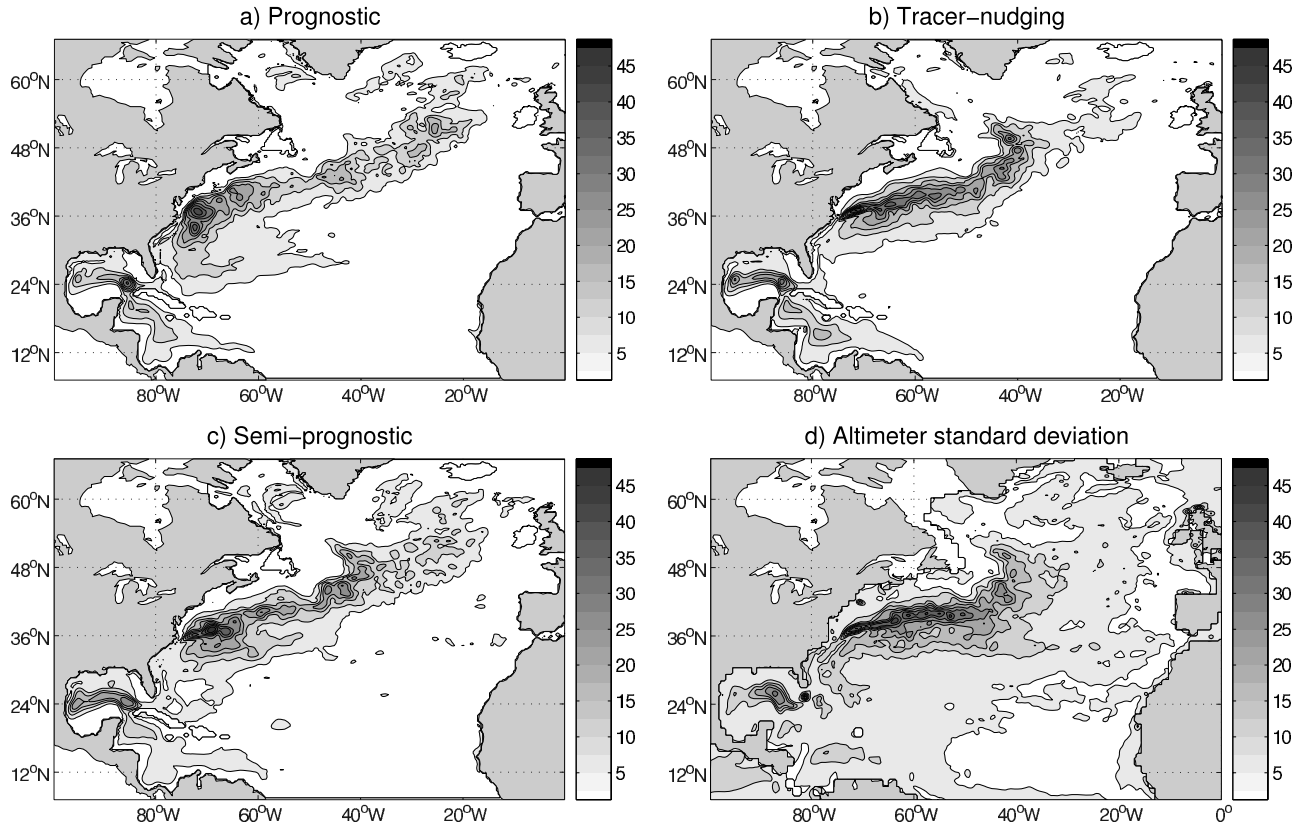

Figure 6. The root-mean-square variability of sea surface height obtained from (a) prognostic, (b) tracer-nudging and (c) semi-prognostic results. (d) Corresponding estimate from altimeter data. The RMS differences between the three model results and the observational result shown in the fourth panel were determined for the whole domain and for a reduced domain covering 40–80W, 30–50N (the Gulf Stream region). The RMS differences are 4.0 (7.7), 3.5 (6.7) and 2.9 (4.8) cm for the prognostic, semi-prognostic and tracer nudged runs, respectively. Numbers in brackets refer to the Gulf Stream sub-domain.

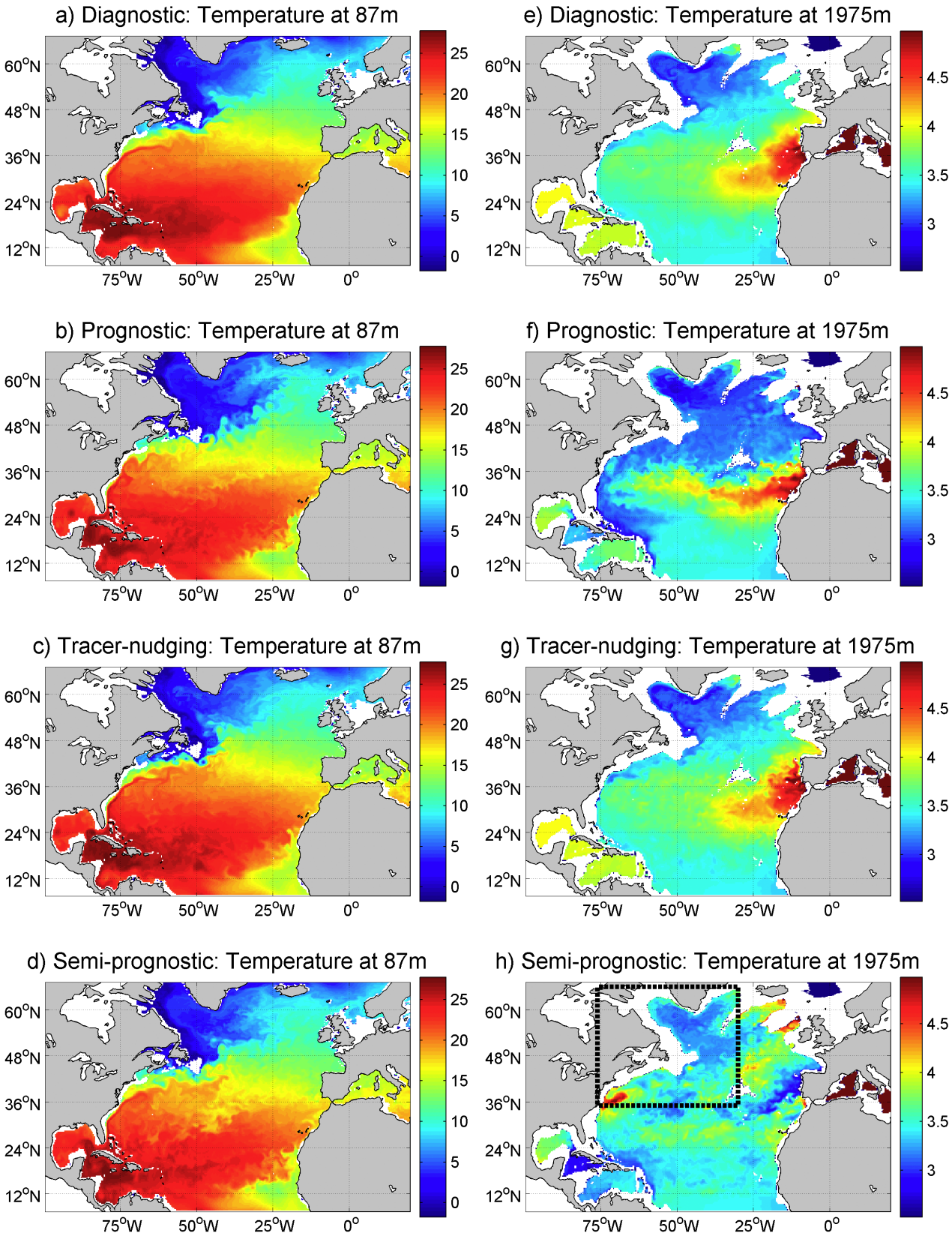

Figure 7. Snapshots of temperature for the diagnostic run from the end of year 15 and the prognostic, tracer-nudging and semi-prognostic model runs from the end of year 30. The left column shows results for layer 6 (87 m), and the right column shows results for layer 16 (1975 m). The box indicated in the northwest portion of Figure 7h indicates the reduced domain considered by *Sheng et al.* [2001].

tional nonlinear terms that depend on $\boldsymbol{u}$, $\boldsymbol{u}_*$ and A_V^*. These nonlinear terms are expected to be small over most of the model domain, but are unlikely to be consistently negligible.

[51] The important point is that we can write $\boldsymbol{u}_{sp} = \boldsymbol{u} + \boldsymbol{u}_*$ where $\boldsymbol{u}_*$ is ultimately determined by the adjustment term in the semi-prognostic momentum equations. If this form is now substituted into the tracer equations, we find that these equations take the form:

$$\frac{\partial T}{\partial t} + \nabla \cdot (\boldsymbol{u} T) = \nabla^2 \left(K_H \nabla^2 T\right) + \frac{\partial}{\partial z}\left(\left(K_V^0 + K_V^*\right)\frac{\partial T}{\partial z}\right) - \nabla \cdot \left(\boldsymbol{u}_* T\right) \tag{7a}$$

$$\frac{\partial S}{\partial t} + \nabla \cdot (\boldsymbol{u} S) = \nabla^2 \left(K_H \nabla^2 S\right) + \frac{\partial}{\partial z}\left(\left(K_V^0 + K_V^*\right)\frac{\partial S}{\partial z}\right) - \nabla \cdot \left(u_* S\right) \tag{7b}$$

where K_V^0 and K_V^* are defined analogous to A_V^0 and A_V^*. Note that (7a) and (7b) are of exactly the same form as (5a) and (5b) but with a special choice of (N^T, N^S) that includes an adjustment to the vertical diffusion plus an advective flux divergence term. Since the change in vertical diffusion enters only through the Richardson number dependence on $\boldsymbol{u}$ and $\boldsymbol{u}_{sp}$, we expect K_V^* to be small compared K_V^0, so the advective flux divergence terms represent the main effect of the adjustment terms in the semi-prognostic equations. The semi-prognostic approach can thus be regarded as a special form of tracer nudging that can be succinctly described as ''advective-nudging''. While this approach has certain appeal [e.g., see *Sheng et al.*, 2001; *Eden et al.*, 2003; *Zhai et al.*, 2004], the specialized nature of the equivalent nudging terms in the tracer equations does limit its range of applicability.

7. Physical Interpretation of the Nudges

[52] We now examine the nudges that result from spectral nudging of the tracer equations. With or without nudging, we expect that under climatological forcing, an equilibrium will eventually be established in which $\langle \overline{T}_{n+1}, \overline{S}_{n+1} \rangle \approx \langle \overline{T}_{n-1}, \overline{S}_{n-1} \rangle$, where the overbar represents an average over several years and the angled bracket represents a spatial smoothing operator. That is, an equilibrium will be achieved in which no further long-term drift occurs. In the absence of nudging, the establishment of this equilibrium requires a balance between the advective and diffusive contributions to the flux divergence (i.e., averaged over a long enough period, the second and third terms on the right side of (5) must balance the first term on the right side). Ideally, this should occur for $\langle \overline{T}, \overline{S} \rangle \approx \langle \overline{T}^{cl}, \overline{S}^{cl} \rangle$, but errors in advection, diffusion or the model forcing can cause this not to be true. The nudging terms are added to ensure that the equilibrium tracer values determined by the model are consistent with the observed climatology. Once the equilibrium state is achieved, the filtered versions of the nudging terms in (5) cancel the net flux divergence that would otherwise cause drift away from the climatology. The long-term average of the nudges simply cancel anomalous flux divergences and hence they must be representable as the sum of advective and diffusive flux divergences, but the separate contributions from each effect are not determined.

[53] We now consider how the nudges added to the model compare with the individual flux divergences associated with advection and diffusion in the model solution. Figure 8 shows time averages over the final five years for the North Atlantic solution obtained with tracer-nudging. The advective flux divergence, the diffusive flux divergence and the temperature nudges are each shown averaged over this same time interval. Note that both the diffusive flux divergence and the nudging term are shown as tracer tendencies, but the advective flux divergence is shown as the negative of the tendency to make it easier to compare with the sum of the other two terms. Ideally, the advective term should be exactly balanced by the diffusive term so that nudges would not be required, but this is clearly not the case.

[54] In the left column of Figure 8, we see that the large-scale structure of the diffusive flux divergence at the upper level is generally consistent with expectations, with cooling to the north and west and warming to the south and east. The diffusive warming at low latitudes, the intense cooling between Cape Hatteras and the Grand Bank and the cooling around the rim of the sub-polar gyre partially balanced the advective tendency, but the imbalance is generally large, particularly in the sub-polar gyre. This imbalance is compensated by the nudging term. Even when averaged across the width of the basin, the nudging term remains significant over most latitudes.

[55] In the right column of Figure 8, we see that the nudging term is required to balance the advective term almost everywhere at the lower level. In fact, from the lower level it appears unlikely that any realistic change in diffusion could provide the divergence required to balance the advection term.

[56] Given that nudging terms are required at depth primarily to balance the heat and salt flux divergences associated with advection, and that it seems unlikely that realistic diffusion could balance these flux divergences, one must ask why these flux divergences exist in a model that is constrained to remain close to climatology. One obvious possibility is that the model advection is simply wrong. As a partial check (beyond checking code), the nudged model runs were each redone with 3rd order upwind differencing replaced by 2nd order centered differencing. The qualitative nature of the model results was not changed, but differences of order 50% were apparent in the nudges. This result emphasizes that when the temperature and salinity are constrained to be near climatology, the heat and salt flux divergences depend quite strongly on the choice of advection scheme. We postulate that errors in advection, rather than diffusion, may be the primary reason for the relatively rapid initial drift of the unconstrained prognostic simulation away from the observed climatological conditions.

[57] From the results discussed above, it seems possible that a different advection scheme could result in substantially reduced advective flux divergences, and hence substantially reduce the need for nudging to maintain the observed climatology. This possibility is consistent with the fact that with similar resolution the DieCAST model, which uses a fourth-order advection scheme, produces stronger deep boundary currents than we have obtained without

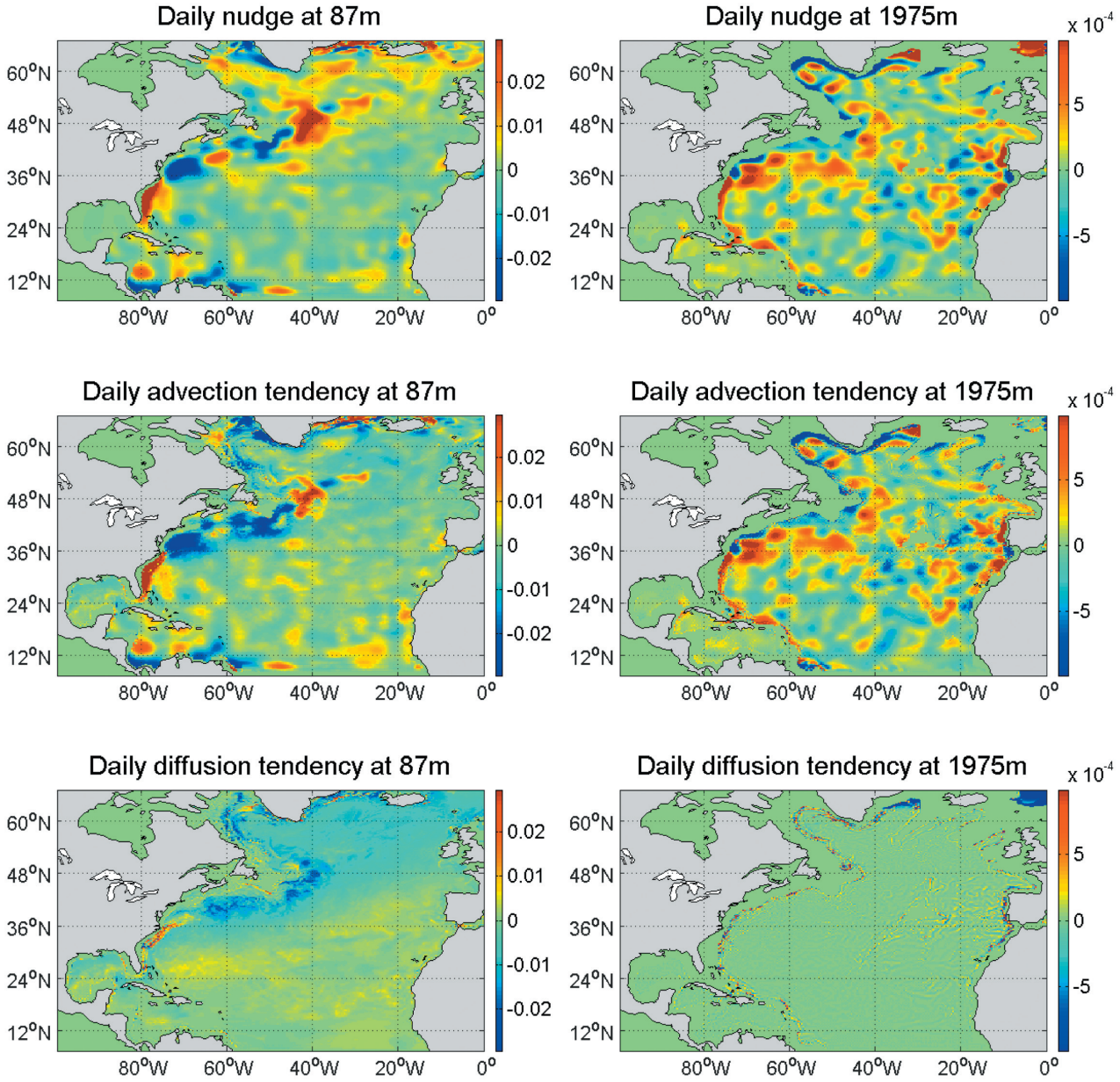

Figure 8. Time-averaged fields for the final 5 years of the 30-year North Atlantic simulation with nudging applied through the tracer equations. The temperature nudges, advective flux divergence and diffusive flux divergence are shown for level 6 in the left column and for level 16 in the right column. In each case, the plots show the change in degrees Celsius that would occur over one day due to the identified term in isolation.

nudging [*Dietrich et al.*, 2004]. *Sheng et al.* [2001] and *Zhai et al.* [2004] use the CANDIE model, a derivative of the DieCAST model that uses a flux limiter [*Thuburn*, 1995] in addition to the fourth-order advection scheme so that small unphysical overshoots are eliminated. As noted in the previous section, their results obtained with the semi-prognostic approach show significantly less drift in the Labrador Sea than our analogous results, which is at least consistent with the above conjecture. Clearly a systematic investigation of the influence of the advection scheme on model results and the need for nudging would be worthwhile.

8. Summary and Discussion

[58] Robust diagnostic results obtained with the POP model, using 1/3rd degree horizontal resolution, driven by NCEP surface fluxes and constrained by the North Atlantic climatology of Yashayaev, give results that are generally

consistent with previous calculations. These results provide a useful indication of climatological conditions in the North Atlantic and a benchmark for evaluation of results of additional integrations. Prognostic model results also agree with previous studies, including their drift from reality for both mean conditions and eddy variability. A large number of experiments were done with modified bottom topography, modified viscosity and diffusion schemes, modified surface boundary conditions and implementation of the topographic stress term associated with the Neptune effect [*Holloway*, 1992], but none of the results were satisfactory. As an alternative to increasing horizontal and vertical resolution we have tested spectral nudging as a way of controlling the model drift.

[59] The primary goal of spectral nudging is to keep the large-scale structures in the modeled seasonal circulation similar to the observed seasonal climatology while permitting the development of realistic variability about this state. This is achieved by nudging in either the temperature and salinity equations (tracer-nudging) or in the momentum equation (the semi-prognostic approach) with the nudges filtered to exclude eddy variability. It is important to recognize that by using this spectral nudging approach, the nudges are restricted to specific frequency bands and they only influence other frequencies through nonlinear interactions.

[60] Both forms of spectral nudging considered here are computationally efficient: in our simulations, the calculations associated with the nudging terms, including the filtering procedures, increased the computational requirements by no more than 25%.

[61] Tracer-nudging prevents model drift by including sources and sinks of heat and salt within the model interior. These artificial sources and sinks may appear to be incompatible with basic conservation principles. However, we note that the evolution of T and S in the ocean model occur through the cumulative effect of flux divergences. Thus, heat or salt that moves out of one cell must appear in an adjacent cell (or exit through the surface or open boundaries) in a physically meaningful way. Since the nudges added to the model compensate for errors in the model's net flux divergences, they must also represent the effect of realizable transports through the model rather than disconnected internal sources and sinks of heat or salt.

[62] While recognizing that the nudges are artificial, they can provide useful insights into the model's deficiencies and thus help improve the models. In particular, examination of the spatial structure of the nudges, and a comparison with the other terms in the tracer evolution equations, suggests that errors in the advection scheme may play an important role in determining the tendency for the model to drift away from the observed climatology. This point warrants further investigation.

[63] For each of the spectral nudging approaches considered here, we have shown that the time-averaged stream functions for both the depth-integrated horizontal circulation and the zonally integrated overturning circulation are maintained close to the robust diagnostic result that is strongly constrained by the observed climatology. Similarly, there is very little drift in the time-averaged temperature and salinity fields for the case in which the temperature and salinity climatologies are nudged directly through the tracer equations. On the other hand, there is considerable drift in our model tracer fields when the semi-prognostic approach is used and the eddy-variability produced by the tracer-nudging approach agrees more closely with observations.

[64] To better understand the differences between the tracer-nudging and the semi-prognostic approach, we have reformulated the latter in terms of nudging in the tracer equations. The result shows that the semi-prognostic approach can be represented as a specialized form of tracer nudging. This is an interesting alternative to the full tracer-nudging approach, but it is clear that it can only correct for problems associated with errors in the model's climatological circulation. The tracer nudging approach corrects for these errors plus others that might occur, including errors in the representation of convective mixing and errors in the mean eddy fluxes that remain after correcting the mean circulation.

[65] We have also shown that the data assimilation approaches discussed here result in significant improvements in the eddy variability as reflected by improved agreement of sea level variability with Topex/Poseiden estimates, particularly in the vicinity of the Gulf Stream. This result was expected since both the energy source required for baroclinic instability and the mean currents and potential vorticity gradients that influence eddy propagation have been maintained. The ability to produce a realistic climatological circulation together with more realistic eddy variability within a common, robust and affordable framework makes the spectral nudging approach a particularly attractive tool for examining the evolution of tracer fields and biological processes.

[66] While the results presented here demonstrate that the spectral nudging approach works in a realistic model simulation, there are still important limitations. One limitation is that the grid resolution used here is merely eddy-permitting and not eddy-resolving. Future work will consider the use of these methods with finer horizontal and vertical resolutions. Note that problems with model drift encountered in model simulations with 1/10th degree horizontal resolution [*Maltrud and McClean*, 2005] indicate the need for such approaches in some applied work even when eddy-resolving models are used. Another concern is that our results depend strongly on the observed climatology and the climatology that we use is obviously influenced by the nature of the data used to determine it. Unfortunately, the Yashayaev climatology (like others) was determined from a collection of data sets that span five decades and some temporal changes are certainly misinterpreted as spatial changes in the mean climatology; our nudging terms will tend to maintain such anomalies. We have used the robust diagnostic approach [*Sarmiento and Bryan*, 1982], with the addition of a spatially varying restoring time and spatial smoothing of the nudging terms, to determine an adjusted climatology that is more consistent with the model dynamics, but still strongly constrained by the observations. This approach has significantly reduced problems with model-data inconsistencies, but it has not eliminated them. Additional methods to improve on estimates of the climatology should be considered.

[67] The most obvious approach to improving the observational estimate of the climatology is to base the estimate on a well-sampled time interval of sufficient duration to define a meaningful climatology. The WOCE observation period offers our best opportunity to do this. For example, it would be worthwhile examining the changes that result from

replacing the climatology of Yashayaev with the recently released WOCE global hydrographic climatology [*Gouretski and Koltermann*, 2004] or analogous products. Another possibility is to combine data sets from different periods with allowance for temporal changes on large spatial scales taken into account. This possibility is under investigation (I. Yashayaev, personal communication, 2005). Such approaches to obtain an improved climatology need to be investigated further in order to take full advantage of the data assimilation approaches considered here.

[68] **Acknowledgments.** We are grateful to the Canadian Foundation for Climate and Atmospheric Sciences for financial support, and the Canadian Foundation for Innovation for infrastructure support. K.R.T. also acknowledges additional financial support from the Discovery Grant program of Natural Sciences and Engineering Research Council of Canada. The Science Strategic Fund of DFO supported collaborative work with Alain Vezina during the development of this method. We also thank Igor Yashayaev for providing free access to his climatology, Greg Lukeman for programming support and Jie Ou for assistance preparing the figures. Jennifer Shore, David Brickman, Charles Hannah, and *JGR* reviewers provided constructive comments that helped clarify the presentation.

References

Barnier, B., L. Siefridt, and P. Marchesiello (1995), Thermal forcing for a global ocean circulation model using a three-year climatology of ECMWF analyses, *J. Mar. Syst.*, *6*, 363–380.

Beckmann, A., C. W. Böning, C. Koberle, and J. Willebrand (1994), Effects of increased resolution in simulating the North Atlantic Ocean, *J. Phys. Oceanogr.*, *24*, 326–344.

Bogden, P. S., R. E. Davis, and R. Salmon (1993), The North Atlantic circulation: Combining simplified dynamics with hydrographic data, *J. Mar. Res.*, *51*, 1–52.

Böning, C. W., W. R. Holland, F. O. Bryan, G. Danabasoglu, and J. C. McWilliams (1995), An overlooked problem in model simulations of the thermohaline circulation and heat transport in the Atlantic Ocean, *J. Clim.*, *8*, 515–523.

Böning, C. W., F. O. Bryan, W. R. Holland, and R. Doscher (1996), Deep-water formation and meridional overturning in a high-resolution model of the North Atlantic, *J. Phys. Oceanogr.*, *26*, 1142–1164.

Böning, C. W., C. Dieterich, B. Barnier, and Y. Jia (2001), Seasonal cycle of meridional heat transport in the subtropical North Atlantic: A model intercomparison in relation to observations near 25N, *Prog. Oceanogr.*, *48*, 231–253.

Chao, Y., A. Gangopadhyay, F. O. Bryan, and W. R. Holland (1996), Modeling the Gulf Stream system: How far from reality?, *Geophys. Res. Lett.*, *23*, 3155–3158.

da Silva, A. M., C. C. Young, and S. Levitus (1994), Atlas of surface marine data, vol. 1, Algorithms and procedures, *NOAA Atlas NESDIS 6*, 83 pp., U.S. Dep. of Commer., Natl. Oceanic and Atmos. Admin., Silver Spring, Md.

Dengg, J., A. Beckmann, and R. Gerdes (1996), The Gulf Stream separation problem, in *The Warmwatersphere of the North Atlantic Ocean*, edited by W. Krauss, pp. 253–290, Gebruder-Borntrager, Stuttgart, Germany.

Dietrich, D. E., A. Mehra, R. L. Haney, M. J. Bowman, and Y. H. Tseng (2004), Dissipation effects in North Atlantic Ocean modeling, *Geophys. Res. Lett.*, *31*, L05302, doi:10.1029/2003GL019015.

Doscher, R., C. W. Böning, and P. Herrmann (1994), Response of circulation and heat transport in the North Atlantic to changes in thermohaline forcing in northern latitudes: A model study, *J. Phys. Oceanogr.*, *24*, 2306–2320.

Ducet, N., P.-Y. Le Traon, and G. Reverdin (2000), Global high resolution mapping of ocean circulation from TOPEX/Poseidon and ERS-1 and -2, *J. Geophys. Res.*, *105*, 19,477–19,498.

DYNAMO Group (1997), Dynamics of North Atlantic models: Simulation and assimilation with high resolution models, *Rep. 294*, 334 pp., Inst. fur Meereskunde and Chritian-Albrechts-Univ., Kiel, Germany.

Eden, C., R. J. Greatbatch, and C. W. Böning (2003), Adiabatically correcting an eddy-permitting model of the North Atlantic using large-scale hydrograpic data: Application to the Gulf Stream and the North Atlantic Current, *J. Phys. Oceanogr.*, *34*, 701–719.

Ezer, T., and G. L. Mellor (1994), Diagnostic and prognostic calculations of the North Atlantic circulation and sea level using a sigma coordinate ocean model, *J. Geophys. Res.*, *99*(C7), 14,159–14,171.

Gerdes, R., and C. Koberle (1995), On the influence of DSOW in a numerical model of the North Atlantic general circulation, *J. Phys. Oceanogr.*, *25*, 2624–2642.

Gouretski, V. V., and K. P. Koltermann (2004), WOCE global hydrographic climatology, *Bundesamt für Seeschifffahrt und Hydrogr.*, no. 35, 52 pp.

Greatbatch, R. J., A. F. Fanning, and A. D. Goulding (1991), A diagnosis of interpentadal circulation changes in the North Atlantic, *J. Geophys. Res.*, *96*, 22,009–22,023.

Holloway, G. (1992), Representing topographic stress for large-scale ocean models, *J. Phys. Oceanogr.*, *22*, 1033–1046.

Klink, J. M. (1995), Thermohaline structure of an eddy-resolving North Atlantic model: The influence of boundary conditions, *J. Phys. Oceanogr.*, *25*, 1174–1195.

Kohl, A., D. Stammer, and B. Cornuelle (2006), Interannual to decadal changes in the ECCO global synthesis, *J. Phys. Oceanogr.*, in press.

Large, W. G., J. C. McWilliams, and S. C. Doney (1994), Oceanic vertical mixing: A review and a model with nonlocal boundary layer parameterization, *Rev. Geophys.*, *32*(4), 363–403.

Lohmann, G. (1998), The influence of a near-bottom transport parameterization on the sensitivity of the thermohaline circulation, *J. Phys. Oceanogr.*, *28*, 2095–2103.

Lu, Y., D. G. Wright, and D. Brickman (2001), Internal tide generation over topography: Experiments with a free-surface z-level ocean model, *J. Atmos. Oceanic Technol.*, *18*, 1076–1091.

Macdonald, A. M. (1998), The global ocean circulation: A hydrographic estimate and regional analysis, *Prog. Oceanogr.*, *41*, 281–382.

Maltrud, M. E., and J. L. McClean (2005), An eddy resolving global 1/10° ocean simulation, *Ocean Modell.*, *8*, 31–54.

Mellor, G. L., C. R. Mechoso, and E. Keto (1982), A diagnostic model of the general circulation of the Atlantic Ocean, *Deep Sea Res.*, *29*, 1171–1192.

Mertz, G., and D. G. Wright (1992), Interpretations of the JEBAR term, *J. Phys. Oceanogr.*, *22*, 301–305.

Pierce, D. W. (1996), Reducing phase and amplitude errors in restoring boundary conditions, *J. Phys. Oceanogr.*, *26*, 1552–1560.

Sarkisyan, A. S., and V. F. Ivanov (1971), The combined effect of baroclinicity and bottom relief as an important factor in the dynamics of ocean currents, *Izv. Acad. Sci. USSR*, 173–188. (*Atmos. Oceanic Phys.*, Engl. Transl.)

Sarmiento, J. L., and K. Bryan (1982), An ocean transport model for the North Atlantic, *J. Geophys. Res.*, *87*, 394–408.

Semtner, A. J., Jr., and R. M. Chervin (1988), A simulation of the global ocean circulation with resolved eddies, *J. Geophys. Res.*, *93*, 15,502–15,522.

Sheng, J., R. J. Greatbatch, and D. G. Wright (2001), Improving the utility of ocean circulation models through adjustment of the momentum balance, *J. Geophys. Res.*, *106*, 16,711–16,728.

Slordal, L. H., and J. E. Weber (1996), Adjustment to JEBAR forcing in a rotating ocean, *J. Phys. Oceanogr.*, *26*, 657–670.

Smith, R. D., M. E. Maltrud, F. O. Bryan, and M. W. Hecht (2000), Numerical simulation of the North Atlantic Ocean at 1/10°, *J. Phys. Oceanogr.*, *30*, 1532–1561.

Smith, W. H. F., and D. T. Sandwell (1994), Bathymetric prediction from dense satellite altimetry and sparse shipboard bathymetry, *J. Geophys. Res.*, *99*, 21,803–21,824.

Smith, W. H. F., and D. T. Sandwell (1997), Global sea floor topography from satellite altimetry and ship depth soundings, *Science*, *277*, 1956–1961.

Stacey, M. W., J. Shore, D. G. Wright, and K. R. Thompson (2006), Modeling events of sea-surface variability using spectral nudging in an eddy permitting model of the northeast Pacific Ocean, *J. Geophys. Res.*, *111*, C06037, doi:10.1029/2005JC003278.

Stammer, D., R. Tokmakian, A. Semtner, and C. Wunsch (1996), How well does a 1/4° global circulation model simulate large-scale oceanic observations?, *J. Geophys. Res.*, *101*, 25,779–25,811.

Thompson, K. R., D. G. Wright, Y. Lu, and E. Demirov (2006), A simple method for reducing seasonal bias and drift in eddy resolving ocean models, *Ocean Modell.*, *13*, 109–125.

Thuburn, J. (1995), Multidimensional flux-limited advection schemes, *J. Comput. Phys.*, *123*, 74–83.

Trenberth, K. (1998), The heat budget of the atmosphere and ocean, in *Proceedings of First International Conference on Reanalysis, WCRP 104*, pp. 17–20, World Clim. Res. Programme, Geneva.

Veronis, G. (1975), The role of models in tracer studies, in *Numerical Models of the Ocean Circulation*, pp. 133–146, Natl. Acad. of Sci., Washington, D. C.

von Storch, H., H. Langenberg, and F. Feser (2000), A spectral nudging technique for dynamical downscaling purposes, *Mon. Weather Rev.*, *128*, 3664–3673.

Webb, D. J., et al. (1991), An eddy-resolving model of the Southern Ocean, *Eos Trans. AGU*, *72*(15), 169–174.

Willebrand, J., B. Barnier, C. Böning, C. Dieterich, P. D. Killworth, C. LeProvost, Y. Jia, J. M. Molines, and A. L. New (2001), Circulation characteristics in three eddy-permitting models of the North Atlantic, *Prog. Oceanogr.*, *48*, 123–161.

Woodgate, R. A., and P. D. Killworth (1997), The effects of assimilation on the physics of an ocean model. Part I: Theoretical model and barotropic results, *J. Atmos. Oceanic Technol.*, *14*, 897–909.

Zhai, X., R. J. Greatbatch, and J. Sheng (2004), Diagnosing the role of eddies in driving the circulation of the northwest Atlantic Ocean, *Geophys. Res. Lett.*, *31*, L23304, doi:10.1029/2004GL021146.

Y. Lu and D. G. Wright, Ocean Circulation Section, Bedford Institute of Oceanography, Dartmouth, Nova Scotia, Canada B2Y 4A2. (wrightdan@mar.dfo-mpo.gc.ca)

K. R. Thompson, Department of Oceanography, Dalhousie University, Halifax, Nova Scotia, Canada B3H 4J1.